ACS APPLIED MATERIALS & INTERFACES

Research Article

www.acsami.org

Tunable Assembly of Vanadium Dioxide Nanoparticles to Create Porous Film for Energy-Saving Applications

Shangjun Ding,[†] Zhanqiang Liu,[†] Dezeng Li,[†] Wei Zhao,[†] Yaoming Wang,[†] Dongyun Wan,[†] and Fuqiang Huang*[,†,‡]

[†] CAS Key Laboratory of Materials for Energy Conversion, Shanghai Institute of Ceramics, Chinese Academy of Sciences, Shanghai 200050, P.R. China

[‡] Beijing National Laboratory for Molecular Sciences and State Key Laboratory of Rare Earth Materials Chemistry and Applications, College of Chemistry and Molecular Engineering, Peking University, Beijing 100871, China

Supporting Information

ABSTRACT: Nanoparticle-assembled vanadium dioxide (VO_2) films have been easily prepared with the assistance of cetyltrimethylammonium vanadate (CTAV) precursor which exhibits self-assembly properties. The obtained VO_2 film has a micro/nano hierarchical porous structure, so its visible-light transmittance is significantly improved (~25% increased compared to continuous film). The VO_2 particle density as well as the film porosity can be facilely controlled by adjusting experimental parameters such as dip-coating speed. Accordingly, film optical properties can also be tuned to a large extent, in particular the visible transmittance (T_{vis}) and near-infrared switching efficiency (ΔT_{nir}). These VO_2 nanoparticle-assembled films prepared by this novel method provide a useful model to research the balance between T_{vis} and ΔT_{nir}.

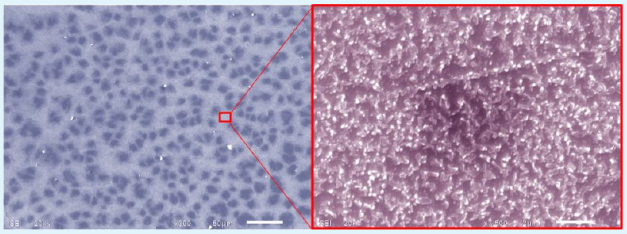

KEYWORDS: *vanadium dioxide, particulate film, self-assembly, porous film, optical controllability*

1. INTRODUCTION

Energy-efficient new constructions have recently aroused great attention due to the global energy crisis, and high-performance windows with proper solar control are the most important components of an energy-efficient building.[1,2] Low-emissivity glass or chromotropic material coatings are widely used to control the heat exchange through windowpanes and depress the room energy consumption.[3−5] Among them, vanadium dioxide (VO_2) is an attractive thermochromic material for smart window applications, because it undergoes a reversible semiconductor/metal (monoclinic/rutile, M/R) phase transition at approximately 68 °C, which simultaneously involves an abrupt change in near-infrared (NIR) transmittance and reflectance.[6−9] This character of VO_2 can be employed to intelligently adjust the NIR-light radiation according to the environment temperature. However, monoclinic VO_2 is a low-band-gap semiconductor (~0.6 eV) and all of its phases have a strong visible-light absorbance,[10] which significantly influences the day lighting of VO_2 coating based windows. To improve the luminous transmittance, ultrathin or porous VO_2 films are highly desirable, but their low mass loadings of VO_2 would, in turn, affect the thermochromic properties. So, in practical windowpane applications, it is necessary to search an optimal balance between the visible-light transmittance and NIR-light control abilities. Nanoparticle-assembled (NPA) film would be a good model to realize this balance, because by changing the assembling density of VO_2 nanoparticles, the film's porosity (i.e., visible transmittance) can easily be adjusted. However, developing tunable synthetic methods to prepare VO_2 NPA films is still a significant challenge.

Currently, most solution methods to prepare porous VO_2 films are based on sol−gel techniques,[11,12] but they have many disadvantages. For example, the traditional molten-V_2O_5 water-quenching method needs more energy consumption and its operation is toxic and unsafe,[13] the vanadium-alkoxide-based process needs expensive precursor and is sensitive to moisture,[14] other polymer-assisted methods have very complicated procedures and control over their porosities is very limited.[15,16] Therefore, a new, simple and safe sol−gel process to prepare VO_2 NPA film with tunable porosity would arouse great interest. To the best of the authors' knowledge, the most effective, common, and reasonable way to fabricate inorganic NPA films is by virtue of phase separation of polymers that was initially added into the precursor sol.[17,18] However, polymer addition may cause some negative effect, such as sol instability, organic residue pollution, and poor film formation. It is therefore necessary to seek an alternative method, that is to synthesize a type of vanadium precursor which many exhibit some self-assembly ability or phase separation effect.

Received: October 17, 2012
Accepted: January 28, 2013
Published: January 29, 2013

Herein, we have successfully developed a facile and controllable sol−gel route to prepare VO_2 NPA films by using an in-house prepared vanadium precursor. The main merits of this novel sol−gel method are listed as follows: (i) the vanadium precursor is easy to prepare, stable and safe to handle; (ii) the vanadium precursor features a long carbon chain, so that it possesses a self-assembly property to assist the formation of NPA film; (iii) VO_2 NPA films prepared by this method have a micro/nano hierarchical porous structure, which significantly enhanced visible-light transmittance; (iv) VO_2 nanoparticle assembling density (i.e., porosity) can easily be tuned by changing the experimental parameters; (v) this VO_2 NPA film provides a good model to study the balance between luminous transmittance and NIR control abilities of thermochromic VO_2 films.

2. EXPERIMENTAL SECTION

2.1. Synthesis of Cetyltrimethylammonium Vanadate (CTAV): a Special Vanadium Precursor. The cetyltrimethylammonium vanadate (CTAV) precursor was synthesized by a simple precipitation reaction.[19] Typically, cetyltrimethylammonium bromide (CTAB, analytical reagent, Sinopharm Chemical Reagent Co., Ltd.) aqueous solution (0.2 M) and ammonium metavanadate (NH_4VO_3, analytical reagent, Sinopharm Chemical Reagent Co., Ltd.) aqueous solution (0.2 M) were mixed together slowly under intense stirring. The obtained white precipitate was filtered, washed with DI water, and absolute ethanol three times each, and then dried at 80 °C for 15 h.

2.2. Preparation of VO_2 NPA Films with the Assistance of CTAV Precursor. The as-prepared CTAV powder was firstly ultrasonically dispersed into *1*-butanol (analytical reagent, Sinopharm Chemical Reagent Co., Ltd.) to form a transparent sol (10 mg/mL), and then vanadium precursor films were prepared by dip-coating CTAV sol onto fused silica substrates at a controlled speed in the range of 5−300 mm/min. After drying at 60 °C for 30 min, the precursor films were annealed at 500 °C in ordinary air for 10−35 min to obtain vanadium pentoxide (V_2O_5) films, and subsequently reduced by H_2/Ar gas (5 bar pressure, 5 vol% of H_2, 430-450 °C for 10−40 min).

2.3. Characterization. Film surface morphologies and roughness were investigated by scanning electron microscopy (SEM, JEOL JSM-6510) and atomic force microscopy (AFM, Dimension 3100 SPM). Film phase identification was performed by X-ray diffraction (XRD, Bruker D8 ADVANCE) with a monochromatized source of Cu $K_{\alpha 1}$ radiation (λ = 0.15405 nm) at 1.6 kW (40 KV, 40 mA). Field-emission transmission electron microscopy (TEM) observations as well as high-resolution transmission electron microscopy (HRTEM) images and selected area electron diffraction (SAED) patterns were collected on a JEOL JEM 2100F microscope working at 200 kV. The Fourier transform infrared spectroscopy (FTIR) information was recorded using Shimadzu IR Prestige-21 instrument in the range of 400-4000 cm^{-1}. The film thickness was measured on a step profiler (Veeco Daktak 150). The thermochromic switching characteristics were monitored on a Hitachi U4100 UV−Vis−NIR spectrophotometer equipped with a bespoke design film heater module in the wavelength range of 240−2500 nm. The temperature was measured using a thermocouple in contact with the films and was controlled through a temperature-controlling unit. Hysteresis loops were measured by collecting the transmittance of films at a fixed wavelength (2500 nm) at an approximate interval of 2.0 °C.

3. RESULTS AND DISCUSSION

3.1. Characterization of Vanadium Precursor. Using the reaction between cationic surfactants and metal polyanions in aqueous solution is an efficient way to prepare special metal precursors that can be potentially applied in the synthesis of mesostructrued metal oxides.[20] In the present study, cetyltrimethylammonium cation (CTA^+) and metavanadate anion (VO_3^-) precipitated to form CTAV precursor, thus its molecule has the same carbon chain as the surfactant of CTAB, which was verified by FTIR measurement (Figure 1a). The two

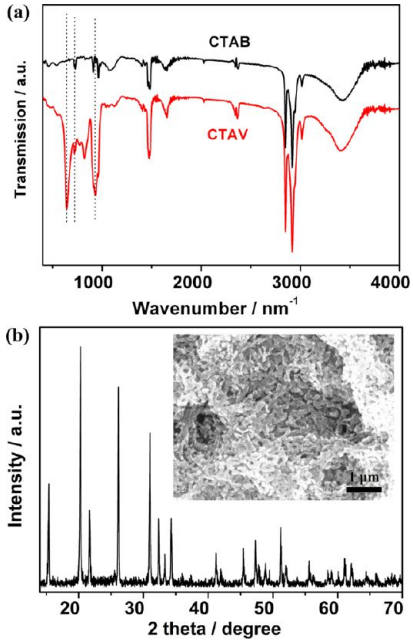

Figure 1. (a) FTIR spectra of CTAV precursor and CTAB surfactant; (b) SEM morphology and XRD pattern of V_2O_5 particles prepared by calcining the CTAV precursor in air at 500 °C for 30 min.

FTIR absorption profiles are very similar except one additional sharp absorption peak at 644 cm^{-1} is observed for CTAV, which is assigned to the vibration of V−O.[21] The absorption band in the range of 1480−1440 cm^{-1} due to the scissoring vibration of $-CH_2-$ and the strong absorption peaks at 2850, 2916, and 3016 cm^{-1} are ascribed to the stretching vibration of $-CH_3$. Other peaks around 930 cm^{-1} may be attributed to the vibration of quaternary ammonium group in the molecule.[22]

However, the organic part of CTAV precursor can be readily burned off in air, producing well-crystallized vanadium pentoxide (V_2O_5, JCPDS No. 41-1426) nanoparticles as shown in Figure 1b. Therefore, if a proper solvent to dissolve CTAV can be found, and then a successive coating-oxidation-reduction process conducted, VO_2 films would most likely result. More importantly, this vanadium precursor that features a long carbon chain in its molecule would have some structure-directing abilities, such as self-assembly or phase separation effect in solution. This means that this surfactant-like precursor can be potentially applied in fabricating nanostructured VO_2 films. Such a method of constructing films through a functional precursor has been rarely reported. In this paper, we have successfully prepared tunable VO_2 nanoparticle-assembled (NPA) films with the assistance of CTAV precursor. The synthetic procedure scheme and the corresponding visual film photographs are shown in Figure S1 in the Supporting Information.

3.2. Morphology and Optical Property of a Typical VO_2 NPA Film. A typical VO_2 NPA film was prepared by dip-coating CTAV/butanol sol onto fused silica substrate (180 mm/min), calcining the precursor film in air (500 °C, 30 min), and then reducing it in a H_2/Ar atmosphere (5 bar pressure, 5 vol% of H_2, 430 °C, 20 min). Figure 2 shows the SEM

dx.doi.org/10.1021/am3023724 | ACS Appl. Mater. Interfaces 2013, 5, 1630−1635

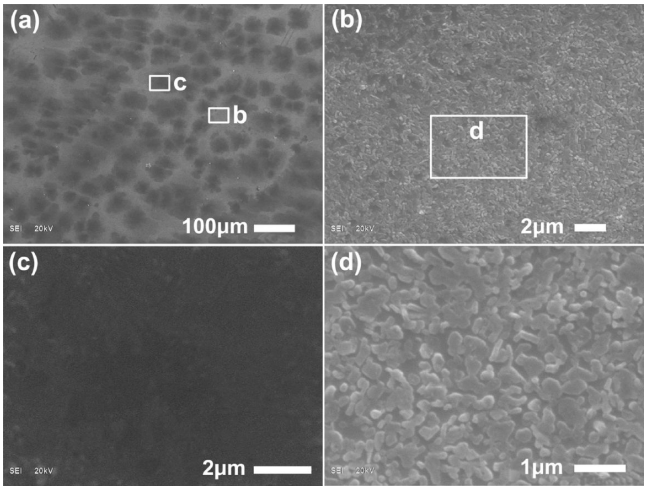

Figure 2. SEM morphology of typical VO_2 nanoparticle-assembled film; the white frame means this area is enlarged for further observation.

morphologies of this typical VO_2 NPA film. Two regions with obvious color contrast are displayed in the wide-view image (Figure 2a), and they are magnified respectively for further observation in Figure 2b, c. The white area is composed of large amount of VO_2 nanoparticles with a diameter range of about 100−500 nm, which is determined by random measurement of 200 particles in the photograph (Figure 2b). A larger magnification image (Figure 2d) indicates that these nanoparticles are discrete, and a nano-scaled porous network exists around them. While in the gray area, fewer particles can be found (Figure 2c) and they actually are micrometer-scaled holes (bare substrate) with size of about 20-50 μm dispersed in film. Therefore, the as-prepared VO_2 film with the assistance of CTAV has a micro/nano hierarchical porous structure, which means a special "light-leak" structure to enhance the visible-light transmittance. Much research focus on the synthesis of nanoporous VO_2 films, however such micro/nano porous film has rarely been reported, and it can be readily achieved in this method by exploiting the structure-directing abilities of CTAV precursor.

The surface morphology of VO_2 NPA film was analyzed by AFM measurements. The typical area in view represents a 5 μm × 5 μm square. According to the AFM topographic image (Figure 3a), nanoparticle-assembled structure is obvious and the particle size was calculated to be in the range of 80−300 nm, which is in good agreement with SEM characterization. Abundant gaps are found in the grain boundaries, revealing that the as-prepared VO_2 film is porous. The uneven particulate nature can be also verified by the rugged height-section profile obtained from line scan (Figure 3b). Because the film is uneven and discrete, it is difficult to determine its thickness. However, some helpful information can still be evaluated from several AFM surface parameters. For example, the difference between the highest peak (Z_{max}) and the deepest valley (Z_{min}) of the image ($R_{p\text{-}v}$ value) is 132.4 nm; the area root-mean-square (RMS) roughness is 17.4 nm, and the region higher than 80 nm and 50 nm account for 18 and 65% of the entire image, respectively.

The cross-section SEM image of this VO_2 NPA film is shown in Figure S2 in the Supporting Information, a rough island-shaped morphology can be clearly observed and its thickness is estimated in the range of 120−200 nm. A step profiler was also

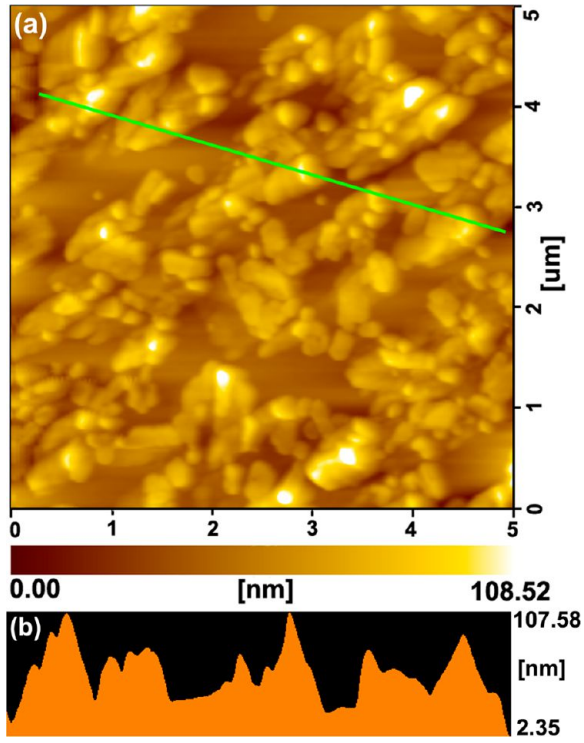

Figure 3. AFM characterization of a typical VO_2 NPA film: (a) topographic image, (b) height-section profile of the marked scanning line in (a).

used to approximately measure the film thickness (see Figure S3 in the Supporting Information). The undulate profile indicates its nanoparticle-assembled structure and an average thickness of about 125 nm was determined from an obvious step. Therefore, if our particulate VO_2 film is continuous, it is much thicker than some other films prepared by traditional sol-gel or sputtering methods.[23,24] As mentioned above, VO_2 has a low band gap, so a thicker VO_2 film would significantly depress the visible-light transmittance. According to the computed results in reference,[25] VO_2 film with a thickness of 120 nm can only have ∼20% luminous transmittance. However, our VO_2 NPA film still possesses a high visible-light transmittance because of its hierarchical porous structure (about 46% according to the following optical analysis).

XRD and TEM measurement were conducted to identify the phase composition and crystal structure of the as-prepared VO_2 NPA film. Slight diffraction peaks at 2θ = 27.8 and 36.9° in the XRD pattern (see Figure S4 in the Supporting Information) suggest the existence of VO_2 (M) phase, which is the functional component of the thermochromic property. Some constituted nanoparticles of the VO_2 NPA film were scraped off for TEM characterization. Irregular shapes with size of about 100−300 nm (Figure 4a) are consistent with the SEM analysis. The SAED pattern (inset in Figure 4b) of an individual particle indicates a single VO_2 (M) crystal and recorded along [001] zone axis. The HRTEM images show clear lattice fringes and the interplanar distances d = 0.428 nm can be indexed to the (010) plane of monoclinic VO_2 (Figure 4c). However, the SAED taken from a wide area shows an intricate pattern (Figure 4d), indicating that the film may contain other impurity vanadium-oxide phases.

Temperature-dependent optical property was measured to study its intelligent light-controlling ability of this typical VO_2

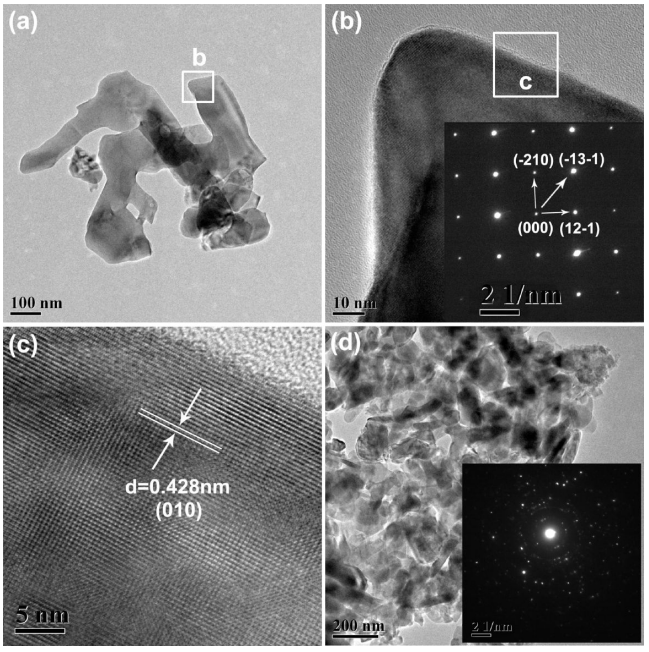

Figure 4. TEM, HRTEM, and SAED characterization of VO_2 nanoparticles from film.

NPA film. Transmittance spectra were recorded in the wavelength range from 0.25 to 2.5 μm at two temperatures (24 and 85 °C) (Figure 5a). There is almost no change in the visible-light range, but noticeable variation occurred in the infrared region when monitored at different temperatures. This

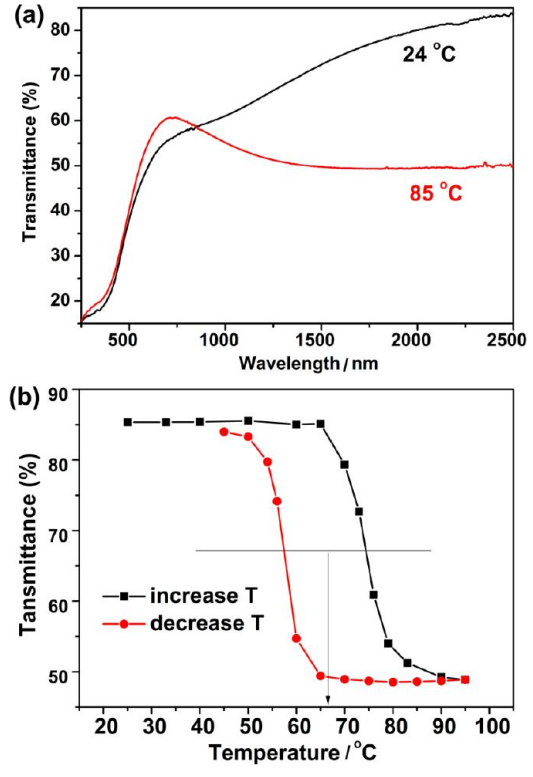

Figure 5. (a) NIR–Vis–UV transmittance of the typical VO_2 NPA film measured at two different temperatures; (b) the corresponding thermal hysteresis loop obtained by monitoring the transmittance of 2500 nm NIR-light.

is the behavior expected from the thermochromic VO_2 material when it undergoes a phase transition from monoclinic to rutile. The integral visible transmittance from 0.38 to 0.78 μm of this "thick" NPA film can reach 46.5% (56% transmittance at 650 nm wavelength), and the infrared transmittance reduction is 34% at 2.5 μm (from 83.4% to 49.4%). This optical property is comparable to other reported results obtained through sputtering deposition or sol–gel method.[26,27]

Thermal hysteresis loop (Figure 5b) was achieved by monitoring the transmittance at 2500 nm during heating and cooling the sample. The IR transmittance decreases gradually with increasing temperature, reaching a minimum value between 70 and 80 °C. Upon cooling down the system, the transmittance increases again, showing a reversible but hysteretic transition. The transition temperature of 66 °C is determined from the midpoint of this hysteresis loop at mean transmittance, and the corresponding loop width of 17 °C is smaller than other reported pure VO_2 films[15,27] Hysteresis narrowing is attributed to the shortage of grain boundaries in our VO_2 NPA film as compared to other dense and continuous films.[28]

3.3. Optical Property Control of VO_2 NPA Films. In the dip-coating process, film thickness or mass loading on the substrate can be readily adjusted by changing the pulling speed. However, if the fabricated film is nanoparticle-assembled rather than continuous, different dip-coating speeds would instead result in different particle-assembling density. This was verified by successfully preparing a series of vanadium-oxide NPA films through our CTAV-assisted method. Figure 6 and Figure S5 in

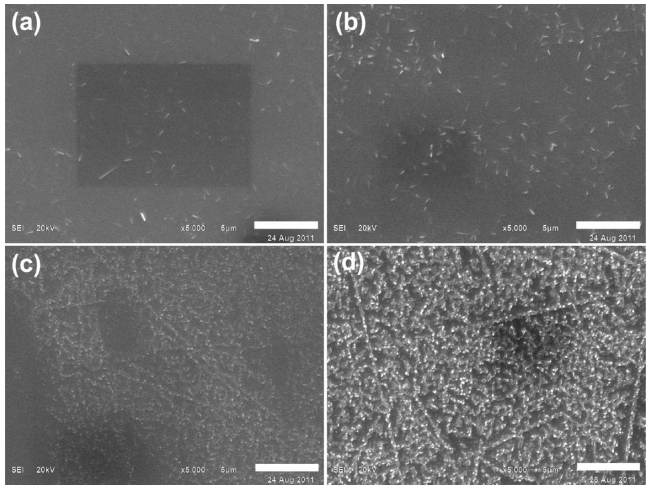

Figure 6. SEM images of V_2O_5 NPA films prepared at different dip-coating speeds: (a) 5, (b) 15, (c) 40, and (d) 80 mm/min. Scale bar: 5 μm.

the Supporting Information depict the SEM morphologies of several V_2O_5 precursor films prepared at different dip-coating speeds. At a low speed (<15 mm/min), discrete island films were produced (Figure 6a, b). Upon raising the dip-coating speed, the nanoparticle assembling density is clearly observed to increase from sparse to dense (Figure 6c, d), and the porous area shrinks gradually until quasi-isolated particles are connected to each other to form a relative continuous film (see Figure S5a–c in the Supporting Information). If the dip-coating speed is too fast to generate a monolayer film, nanoparticles would accumulate upwards to form much thicker films (see Figure S5d in the Supporting Information). The

dx.doi.org/10.1021/am3023724 | ACS Appl. Mater. Interfaces 2013, 5, 1630–1635

corresponding transmission spectra of these V_2O_5 particulate films are illustrated in Figure S6 in the Supporting Information. It is clear that the film transmittance can be easily tuned by changing the dip-coating speed (i.e., particle density), and high visible-light transmittance is ensured by reducing the assembling density suitably.

In addition, the micro/nanohierarchical porous structure of this NPA film is also closely related to the dip-coating speed. When constituent particles apart distantly because of less mass loading, micrometer-scaled holes cannot be distinguished clearly. While the dip-coating speed reaches 40 mm/min, some big pores begin to emerge (Figure 7a), and they become

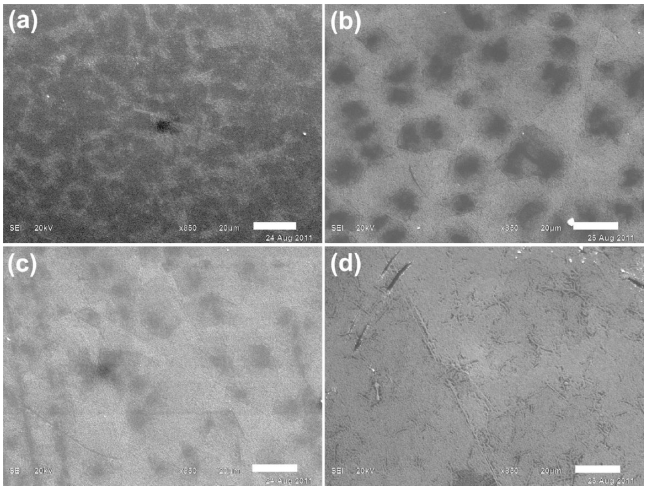

Figure 7. SEM morphologies of several V_2O_5 NPA films prepared at different dip-coating speeds: (a) 40, (b) 160, (c) 200, and (d) 300 mm/min. Scale bar: 20 μm. The dark area is the micrometer-sized pores.

more obvious as the dip-coating speed increases. A typical hierarchical porous structure can be obtained at 160 mm/min as shown in Figure 7b and Figure S7 in the Supporting Information. But if the dip-coating speed was much too large, these micrometer holes would be filled in with vanadium-oxide nanoparticles as well because of more mass loading (Figure 7c, d). The basic framework of this micro/nanohierarchical porous structure can be reserved after the reduction treatment, although particle shape and size may cause subtle changes.

On the basis of the facile control of particle density and film porosity, the optical properties of these particulate VO_2 films can also be adjusted in a large extent. We use the integral visible (0.38−0.78 μm) transmittance (T_{vis}) and the near-infrared (2500 nm) transmittance change after M/R phase transition (ΔT_{nir}) as two key parameters to assess the optical properties of VO_2 NPA films. All the transmission spectra of different VO_2 films were measured at two temperatures (24 and 85 °C) in Figure 8. As expected, higher VO_2 particle density (i.e., faster dip-coating speed) results in lower visible-light transmittance (T_{vis}), but facilitates the enhancement of thermochromic properties (optical switching efficiency, ΔT_{nir}). This rule can be more clearly reflected in Figure 9a, where the T_{vis} and ΔT_{nir} variation with the dip-coating speed is plotted. For example, the sample prepared at a maximum dip-coating speed (300 mm/min) possesses the largest value of ΔT_{nir} (45.0 %), but has a minimum of 40.2 % visible transmittance (T_{vis}). A large number of experiments were performed to tune ΔT_{nir} and T_{vis} by changing the particle density, and all the (ΔT_{nir}, T_{vis}) values are

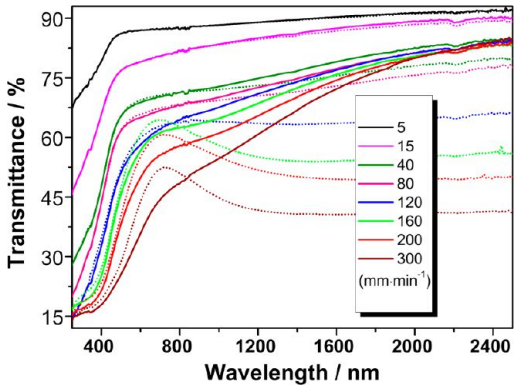

Figure 8. Transmittance switching properties of diverse VO_2 nanoparticle-assembled films prepared at different dip-coating speeds. Solid line (24 °C) and dot line (85 °C).

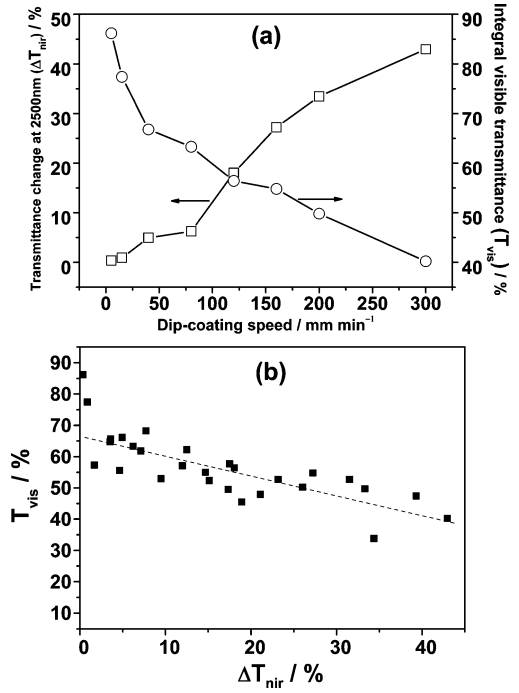

Figure 9. (a) Integral visible transmittance (T_{vis}) and transmittance change at 2500 nm (ΔT_{nir}) of diverse VO_2 NPA films prepared at different dip-coating speeds; (b) the relationship between T_{vis} and ΔT_{nir} for different nanoparticle assembling density.

plotted in one coordinate diagram (Figure 9b). It was found that quasi-linear relationship can be fitted between T_{vis} and ΔT_{nir}: the eliminating T_{vis} and the growing ΔT_{nir}. Such intentional particle density adjustment implies that the VO_2 NPA film prepared by this CTAV-based method provide a useful model to research the balance between T_{vis} and ΔT_{nir} for practical application.

The reflectance spectra of various VO_2 NPA films were also studied in Figure S8 in the Supporting Information. Interestingly, it is worth noting that the film obtained at an appropriate dip-coating speed (e.g., 15 mm/min) exhibit a minimum reflectivity, which is even lower than bare glass substrate. So we deduced that proper nanoparticle-assembled structure may have some self-antireflection phenomenon, which inspired us to developing functional coatings by designing new nanostructures.

dx.doi.org/10.1021/am3023724 | ACS Appl. Mater. Interfaces 2013, 5, 1630−1635

4. CONCLUSION

A novel and facile sol-gel route has been successfully developed to prepare VO_2 nanoparticle-assembled (NPA-) films with the assistance of an in-house prepared vanadium precursor: cetyltrimethylammonium vanadate (CTAV). The particular self-assembly properties of CTAV precursor determine the final morphology of VO_2 film, and micro/nano hierarchical porous structures were fabricated, which significantly enhanced the visible-light transmittance. In addition, VO_2 particle assembly density (*i.e.* film porosity) was easily tuned by changing the dip-coating speed, so accordingly, the film optical properties such as visible transmittance (T_{vis}) and near-infrared switching efficiency (ΔT_{nir}), can also be adjusted to a significant extent. This CTAV-based method has been proven to be an effective way to build VO_2 NPA films and to balance their T_{vis} and ΔT_{nir} for practical applications.

■ ASSOCIATED CONTENT

Supporting Information

More characterization, including SEM images, step profile, XRD pattern, transmittance, and reflectance spectra of nanoparticle-assembled vanadium-oxide films. This material is available free of charge via the Internet at http://pubs.acs.org.

■ AUTHOR INFORMATION

Corresponding Author

*E-mail: huangfq@mail.sic.ac.cn and huangfq@pek.edu.cn. Tel: +86-21-5241-1620. Fax: +86-21-5241-6360.

Notes

The authors declare no competing financial interest.

■ ACKNOWLEDGMENTS

This work was financially supported by National 973 Program of China Grant 2009CB939903, NSF of China Grant 91122034, NSF for Distinguished Young Scholars of China 51125006, NSF of Shanghai Grant 51121064, Innovation Program of the CAS KJCX2-EW-W11, and the CAS/SAFEA International Partnership Program for Creative Research Teams.

■ REFERENCES

(1) Gieseler, U. D. J.; Heidt, F. D.; Bier, W. *Renew. Energy* **2004**, *29*, 369−376.
(2) Khudhair, A. M.; Farid, M. M. *Energy Convers. Manage.* **2004**, *45*, 263−275.
(3) Jin, Z. C.; Hamberg, I.; Granqvist, C. G.; Sernelius, B. E.; Berggren, K. F. *Thin Solid Films* **1988**, *164*, 381−386.
(4) Svensson, J. S. E. M.; Granqvist, C. G. *Appl. Phys. Lett.* **1986**, *49*, 1566−1568.
(5) Chiba, K.; Takahashi, T.; Kageyama, T.; Oda, H. *Appl. Surf. Sci.* **2005**, *246*, 48−51.
(6) Woodley, S. M. *Chem. Phys. Lett.* **2008**, *453*, 167−172.
(7) Allen, P. B.; Wentzcovitch, R. M.; Schulz, W. W. *Phys. Rew. B* **1993**, *48*, 4359−4363.
(8) Wu, C. Z.; Dai, J.; Zhang, X. D.; Yang, J. L.; Qi, F.; Gao, C.; Xie, Y. *Angew. Chem., Int. Ed.* **2010**, *49*, 134−137.
(9) Sohn, J. I.; Joo, H. J.; Porter, A. E.; Choi, C. J.; Kim, K.; Kang, D. J.; Welland, M. E. *Nano Lett.* **2007**, *7*, 1570−1574.
(10) Maruyama, T.; Ikuta, Y. *J. Mater. Sci.* **1993**, *28*, 5073−5078.
(11) Partlow, D. P.; Gurkovich, S. R.; Radford, K. C.; Denes, L. J. *J. Appl. Phys.* **1991**, *70*, 443−452.
(12) Guzman, G.; Beteille, F.; Morineau, R.; Livage, J. *J. Mater. Chem.* **1996**, *6*, 505−506.
(13) Hanlon, T. J.; Coath, J. A.; Richardson, M. A. *Thin Solid Films* **2003**, *436*, 269−272.
(14) Beteille, F.; Livage, J. *J. Sol−Gel Sci. Technol.* **1998**, *13*, 915−921.
(15) Kang, L. T.; Gao, Y. F.; Luo, H. J. *ACS Appl. Mater. Interfaces* **2009**, *1*, 2211−2218.
(16) Du, J.; Gao, Y. F.; Luo, H. J.; Kang, L. T.; Zhang, Z. T.; Chen, Z.; Gao, C. X. *Sol. Energy Mater. Sol. Cells* **2011**, *95*, 469−475.
(17) Luo, M.; Cheng, K.; Weng, W. J.; Song, C. L.; Du, P. Y.; Shen, G.; Xu, G.; Han, G. R. *Nanoscale Res. Lett.* **2009**, *4*, 809−813.
(18) Luo, M.; Cheng, K.; Weng, W. J.; Song, C. L.; Du, P. Y.; Shen, G.; Xu, G.; Han, G. R. *Mater. Lett.* **2008**, *62*, 1965−1968.
(19) Luca, V.; Maclachlan, D. J.; Hook, J. M.; Withers, R. *Chem. Mater.* **1995**, *7*, 2220−2223.
(20) Ciesla, U.; Demuth, D.; Leon, R.; Petroff, P.; Stuky, G.; Unger, K.; Schüth, F. *J. Chem. Soc., Chem. Commun.* **1994**, 1387−1388.
(21) Voronkov, M. G.; Shergina, N. I.; Lapsin, A. F. *Bull. Acad. Sci. USSR Div. Chem. Sci.* **1972**, *21*, 2745−2746.
(22) Frederickson, L. D., Jr.; Hausen, D. M. *Anal. Chem.* **1963**, *35*, 818−827.
(23) Xu, G.; Jin, P.; Tazawa, M.; Yoshimura, K. *Appl. Surf. Sci.* **2005**, *244*, 449−452.
(24) Kang, L. T.; Gao, Y. F.; Chen, Z.; Du, J.; Zhang, Z. T.; Luo, H. J. *Sol. Energ. Mat. Sol. C.* **2010**, *94*, 2078−2084.
(25) Kang, L. T.; Gao, Y. F.; Luo, H. J.; Chen, Z.; Du, J.; Zhang, Z. T. *ACS Appl. Mater. Interfaces* **2011**, *3*, 135−138.
(26) Mlyuka, N. R.; Niklasson, G. A.; Granqvist, C. G. *Appl. Phys. Lett.* **2009**, *95*, 171909.
(27) Lu, S.; Hou, L.; Gan, F. *J. Mater. Sci. Lett.* **1996**, *15*, 856−857.
(28) Kim, D. H.; Kwok, H. S. *Appl. Phys. Lett.* **1994**, *65*, 3188−3190.